Cosine-type Absorbing Optical Potential for the Modeling of Quantum Dynamics with the Fourier Grid and Optimizer Packages

© *Vladimir B. Sovkov* [1,2], *Jizhou Wu* [2], *and Jie Ma* [2]

[1] St. Petersburg State University, 7/9 Universitetskaya nab., St. Petersburg 199034, Russia
[2] State Key Laboratory of Quantum Optics and Quantum Optics Devices, Institute of Laser Spectroscopy, Shanxi University, Taiyuan 030006, China

e-mail: v.sovkov@spbu.ru, wujz@sxu.edu.cn, mj@sxu.edu.cn

In order to model the spectroscopic and scattering properties of a quantum system, we propose and explore a new absorbing complex-type optical potential based on a combination of cosine functions. This function provides a high degree of smoothness to joint with a physical real-type potential. The capabilities of this function are investigated in terms of its effect on otherwise freely evolving quantum dynamics. We use our open-source programs to implement the Fourier Grid method with the Optimizer package (in Matlab), freely available at https://sourceforge.net/projects/optimizer-sovkov/.

Keywords: quantum dynamics; damping boundary conditions; optical potential; Fourier Grid method; spectroscopy of ultracold ensembles.

1. Introduction

The time-dependent and time-independent Schrödinger equations [1] have always been a particular focus of theoretical and computational physics and chemistry, and many efficient methods, algorithms, and computer programs for solving these have been developed. However, since they form the basis of non-relativistic quantum mechanics and can pave the way for quantitatively accurate descriptions and prognoses of the most promising modern experiments, numerical solutions to these equations are of great interest, and this is expected to be the case for the foreseeable future.

New experimental targets and techniques have given rise to new requirements for these methods and programs. For example, in recent years, spectroscopy of the photoassociation (PA) of ultracold atoms (e. g., [2–4] and references therein) have drawn substantial attention, since these experiments are expected to be able to produce molecular ensembles in exotic states (and to some extent have already done so), such as molecules in their absolute (i. e., in all degrees of freedom) ground states [5,6], quantum gases and liquids of these molecules [7–9], and so on. Besides the obvious interest in these systems from a fundamental physics standpoint, they appear to be very prospective in applications in fields such as fully controlled quantum chemical reactions [10], highly precise measurements [11–13], and the development of quantum computers and quantum information systems [14,15].

Probably the most efficient way to enhance the PA process, and hence to increase the production of such ensembles, is by using magnetically tuned near-dissociation Feshbach resonances [16–19].

The Feshbach resonances belong to the continuous spectrum, and those of interest here lie within a range of very low energies (the typical temperatures of ultracold gases of atoms can be $\sim 1\,\mu$K and lower). A wavepacket on the continuous spectrum evolves within an infinite range of spatial coordinates, which of course cannot be strictly represented numerically. One way to overcome this difficulty is by the introduction of artificial absorbing boundary conditions or optical potentials [20], in order to damp the wavepacket amplitudes at the boundaries of the physically important spatial interval. The efficacy of this damping depends on the type of absorbing function and the length of its action: this length must not be much less than the length of the oscillation of the plane wave (de Broglie wavelength) with the energy of interest. Low-energy Feshbach resonance states have exceptionally long wave oscillations (hundreds of Bohr radii or more), which requires the use of very long damping zones. An examination of the various types of absorbing functions and ways of applying them can help to reduce the volume of these zones, or at least to estimate the expectation values of the computational errors of such reductions.

In the whole, the resonance phenomena, including the Feshbach resonances, are among the most exciting topics in various fields of quantum physics and chemistry, such as the scattering theory, spectroscopy, and so on, in which absorbing functions are highly-demanded.see the literature referred to in the following section (Sec. 2.1 — „Basic physics and algorithms").

The principal aims of the present work were as follows:

− To describe a trigonometric (cosine)-type absorbing function, which to the best of our knowledge has never before been used in this type of problem.

– To introduce and briefly describe our computer program for solving the 1-D multichannel Schrödinger equations using the (Mapped) Fourier Grid method, which is adapted for use with our Optimizer package (in Matlab), [21].

To carry out a numerical investigation of the properties and capabilities of the cosinetype absorbing function, with the help of our Fourier Grid program. In part, we explore an ability of our new absorbing function to provide reasonable description of quantum dynamics employing short-range absorption zones (comparable or shorter than the de Broglie wavelength), with the prospect of simulating Feshbach resonances of atomic pairs with reasonable computational expanses but without a crucial loss of the accuracy.

All the computer programs used in our work are described and made available for a free download (see Ref. [21] and Sec. 4 below).

In the course of our investigation, we found a relatively recent work [22], which also dealt with an absorbing function constructed from cosines and applied it in optimal control theory calculations. Although the authors of [22] did not provide all the details on this function promising to give them in a separate publication later, it is clear from the context that it strongly differs from the one described in the present paper. Contrary to our approach, they constructed its imaginary part as a negative square of finite cosine series and its real part as other finite cosine series, and optimized the coefficients to minimize the transmission and reflection; no smoothness conditions at the joint points, which are essential in our work, were analyzed. We hope that both approaches will find their use without contradicting each other. On the other hand, the very fact of publishing the cited paper testifies the regrown current interest to the absorbing functions and optical potentials (despite a long history of the question) thanks to new developments in many fields, including the optimal control theory as in Ref. [22] and the spectroscopy of ultracold ensembles as in the present paper.

We understand that, although for the present results on the cosine-type absorbing function the use of our programs on the Fourier Grid method was essential, there may be readers interested in only physical aspects and those interested in only software. The former ones can ignore Sec. 4 „Software implementation" without lacking the physical picture, while the latter ones can concentrate their attention on this Sec. 4 along with the program manuals referred to from there, ignoring other materials.

2. Methods

2.1. Basic physics and algorithms

As is well known [1], all the principal properties of a quantum system are determined by the time-independent (stationary) and time-dependent Schrödinger equations.

Many efficient algorithms for solving the Schrödinger equations have previously been proposed (e.g., see [23–25] and references therein). In the present work, we

employ one of these, which is known as the Fourier Grid method [26–32]. Our realization of this method as a software program is described in Sec. 4 „Software Implementation" below. These programs can be freely downloaded from [21]. Along with the programs, the English- and Russian-language manuals are provided, where the algorithm and the underlying physics are detailed.

When the (presumably oscillatory) dynamics of the wavepacket occur entirely within the field of a bound potential in a closed domain, no substantial extra difficulties arise; however, problems emerge when computation of a free (decaying, dissociating) state dynamics is needed, such as when modeling molecular predissociation spectra or Feshbach resonances in scattering theory. In this case, the wavepacket reaches the rightmost boundary of the computational grid within a limited time, and due to the periodic character of the Fourier transform, intrudes into (or is reflected from) the spatial domain at the opposite leftmost boundary, producing non-physical features in the computational results. In Fourier transform theory, this effect is known as „aliasin". A straightforward method of expanding the computational grid so that the wavepacket does not reach the boundary within the necessary computational time (which would also ensure a satisfactory density of the computed pseudo-bound states) has the obvious drawback of an unreasonable increase in the necessary computational resources (although this is possible to some extent in the framework of the Mapped Fourier Grid algorithm).

Possible solutions to this problem include the introduction of absorbing boundary conditions or the so-called optical potential. In the first approach, the wavefunction (packet) at each subsequent time step is multiplied by a function, which is actualized within a certain vicinity of the boundary and decreased towards it.the absorbing function.thus preventing the packet from reaching this boundary. In the second approach, a negative imaginary-type summand (or a more general complex-type one.see below) is added to the potential function U itself, ensuring that $\exp\{-(i/\hbar)U\delta t\}$ (where δt is the elementary time step in the step-by-step scheme) behaves analogously, i.e., it is actualized within a certain vicinity of the boundary and decreases towards it. These approaches are practically equivalent up to the logarithm or exponent operations; however, the optical potential method is somewhat more general, since the absorbing function can be only applied when the dynamics are computed in a step-by-step way, which is not always the case. Physically, the absorbing barrier retains the ability to transmit and reflect some part of the wavepacket, and the parameters of this barrier should be adjusted so that the transmission and reflection coefficients are minimal.

Various forms of the absorbing functions or optical potentials have been proposed and analyzed. A comprehensive review of the relevant works published before 2004 is presented in [20], some of which [33–39] are mostly relevant to our investigation (notice that Ref. [39] was missed in Ref. [20]). A few examples of more recent works on the subject can be found in [22,40–44]. We would also like

to mention the works [45–48] exploring the subject of the artificial boundary conditions but from somewhat different points of view (the complex scaling technique, the Green functions technique).

It was discovered [20,33,34] that the properties of the absorbing function are controlled by the single master parameter of the length $\lambda = 2\pi\hbar/\sqrt{2mE}$ of the oscillation of a plane wave (de Broglie wavelength) with energy E. In other words, they are universally expressed in dimensionless relative units of E and λ. This observation has been used in many works (e. g., [33,34]), where the results of numerical tests with some optical potentials for a particular model brought forth a kind of general multipurpose recommendations.

An interesting practical generalization of the concept of the optical potential has been considered in several works [20,36,37]. If the efficiency of an optical potential is optimized for a certain specific energy E_0, it loses efficiency for other energies, and especially those that are noticeably lower than E_0. The reason for this behavior is rather obvious: the spatial range of an efficiently absorbing optical potential must be no noticeably less than the oscillation length of the wavefunction, since otherwise the wavefunction would not register the existence of this barrier. On the other hand, the part of the wavefunction in the absorbing zone has nothing to do with the actual physics of the process, and we are able to warp this in any way that is convenient for us. The effective oscillation length of a low-energy wavefunction can be decreased by introducing, along with the absorbing imaginary-type potential, a real-type summand to reduce the potential function in this region to an appropriate value, to form a complex-type optical potential.

2.2. Trigonometric (cosine-type) absorbing function and optical potential

In our programs, we use absorbing boundary conditions and an optical potential, as described below. It is clear that any alternative or additional optical potential can be introduced in any coordinate region at the construction stage of the potential function.

We attempted to fulfill the requirement that the function should be as smooth as possible, meaning that the maximum possible number of several lower-order derivatives at the points of joining should be continuous. The evolution operator is in fact a complex differentiation operator; it was shown in Ref. [34] that the semiclassical reflection coefficient remains zero up to the order of the WKB approximation that is equal to the order of the maximal continuous derivative at the front of the optical potential. Trigonometric functions have well-understood smoothness properties and their combinations look prospective to ensure this requirement.

In our work, we chose an absorbing function in the form:

$$f_{k\beta}(z(r)) = \left[\frac{1}{2} + \sum_{n=1}^{k} c_n \cos\left((2n-1)\pi z(r)\right)\right]^{\beta}, \quad (1)$$

Table 1. Coefficients c_n in combinations Eq. (1) of k cosines, ensuring the continuity of the derivatives of orders up to $2k - 1$

k	c_1	c_2	c_3	c_4
1	1/2	–	–	–
2	9/16	−1/16	–	–
3	75/128	−25/256	3/256	–
4	1225/2048	−245/2048	49/2048	−5/2048

where r is the spatial coordinate and

$$z(r) = \frac{r - \min(r)}{\max(r) - \min(r)},$$

if a decrease in the function is desired towards the right boundary, or

$$z(r) = \frac{\max(r) - r}{\max(r) - \min(r)},$$

if a decrease in the function is desired towards the left boundary; $\min(r)$ and $\max(r)$ designate the left and right points in the r-scale, where the lower-order derivatives of the function Eq. 1 should turn to zero (see below).

It is obvious that, at least for $\beta = 1$, this function automatically ensures that all the derivatives of odd orders are zero at the ends of the region, $z \in [0, 1]$. The derivatives of the even orders are:

$$\frac{d^{2q} f_{k1}(z)}{dz^{2q}} = \frac{1}{2}\,\delta_{q0}$$

$$+ (-1)^q \sum_{n=1}^{k} c_n \left((2n-1)\pi\right)^{2q} \cos\left((2n-1)\pi z(r)\right). \quad (2)$$

Hence, all the derivatives of orders up to $2k - 1$ are zero at both ends of the interval when the following equations are satisfied:

$$\sum_{n=1}^{k} c_n = 1/2, \qquad \sum_{n=1}^{k} c_n(2n-1)^{2q} = 0, \quad (3)$$

where $q = 1, 2, \ldots, k - 1$.

The coefficients c_n that are important in practice were found from the solutions of these equations, as listed in Table 1. Based on our experience, cases with $k > 4$ do not need to be considered, due to the limited accuracy of digital computations; however, they can be computed in our programs.

For $\beta \neq 1$:

$$f_{k\beta}(\delta z) \sim \left[1 - (\delta z)^{2k}\right]^{\beta} \sim 1 - \beta(\delta z)^{2k},$$

$$f_{k\beta}(1 - \delta z) \sim \left[(\delta z)^{2k}\right]^{\beta} = (\delta z)^{2k\beta},$$

and consequently the derivatives of the same order of up to $2k - 1$ remain zero at the leading edge, while at the falling

edge the derivatives are zero up to the order of $2k\beta - 1$; for $\beta > 1$, this increases the degree of smoothness of the function at the falling edge. The use of the function

$$\tilde{f}_{k\beta}(z) = (1 - f_{k\beta}(1 - z)) \tag{4}$$

means that this property is fulfilled at the leading edge.

To ensure the consistent transformation of the absorbing function to the optical potential and vice versa, the parameter β should be expressed in the form

$$\beta = \alpha E_0 \frac{\delta t}{\hbar}, \tag{5}$$

where E_0 is some reference energy, and α is an adjustable, dimensionless, linear factor in the optical potential with the form:

$$V_{k\alpha}^{Oi}(r) = i\alpha E_0 \ln\left(f_{k1}(z(r))\right). \tag{6}$$

The same mathematics is very suitable for the real-type (lowering) part of the complex-type optical potential. We use:

$$V_{k\gamma}^{Or}(r) = \gamma E_0 \left(f_{k1}(z(r) - 1)\right), \tag{7}$$

(where γ is an adjustable dimensionless parameter) with the total optical potential

$$V_{k\alpha\gamma}^{O}(r) = V_{k\alpha}^{Oi}(r) + V_{k\gamma}^{Or}(r). \tag{8}$$

In terms of the optical potential, the smoothness properties at the leading edge, which are most interesting to us, are the same as for the absorbing function itself.

We notice in passing that the Eqs. (1) and (4) can be used for many other purposes, e.g., in numerical differentiation using the Fourier transform method or for the smooth connection of dependencies in a way that is similar to but in some sense more general than the spline method.

3. Results

Below, we present numerical tests of the properties of the absorbing functions (optical potentials) of the form described in Section 2.2 .Trigonometric (cosine-type) absorbing function and optical potential., using our Fourier Grid programs (see Ref. [21] and Sec. 4 below). We simulate computations of a straightforward quantum dynamics (which would be a freely evolving case if no absorbing function were included) using the model of Vibók and Balint–Kurti [33] and a modified (and in our opinion, more practical) similar model.

In [33], Vibók and Balint–Kurti proposed a convenient computational model for exploring the properties of various optical potentials, and applied it to a set of such potentials (powers and exponents of $1/r$). The recommendations set out in Ref. [33] have been adopted by many researchers since then.

In their model, a Gaussian wavepacket with mean energy E was evolved in the field of a constant (conventionally zero) potential, until it reached the absorbing barrier formed

by an optical potential located within a limited range of the spatial coordinates of length $l\lambda_0$ around the center of the overall range (λ_0 is the de Broglie wavelength, l is the user-defined dimensionless length of the absorbing zone). It was partly reflected from the region in front of the barrier and partly transmitted to the region behind it. After sufficient time t for both parts of the wavepacket $\psi(r, t)$ to reach regions far from both the barrier and the computational grid boundaries, the reflection $R = \int_{\{r_-\}} |\psi(r, t)|^2 dr$ and transmission $T = \int_{\{r_+\}} |\psi(r, t)|^2 dr$, coefficients were estimated, where $\{r_-\}$ and $\{r_+\}$ denote the spatial regions in front of and behind the barrier. Most of the test computations were done for an evolving Gaussian wavepacket with mean energy $E = E_0 = 0.1$ au and mass $m = 1836.18$ au (where the atomic Hartree units (au) were used). The spatial span $l\lambda_0$ of the absorbing zone was varied from $l = 1$ to $l = 15$, and the „optimal" parameters of the optical potentials were determined in order to minimize the sum $(R + T)$ for this reference energy $E_0 = 0.1$ au with the de Broglie wavelength λ_0.

Some of our test computations were done using the exact model of Vibók and Balint–Kurti but with our optical potential, as described in Section 2.2 „Trigonometric (cosine)-type absorbing function and optical potential". Fig. 1 illustrates the evolution of the wavepacket in this model, computed with our Fourier Grid package (notice the logarithmic scale for the amplitudes of the wavepacket). The reflected and transmitted parts of the wavepacket are clearly distinguishable.

We also considered another model (in our opinion a more practical one), in which we placed an absorbing region near the rightmost boundary, and added a wall near the leftmost boundary with the maximum amplitude of $100E$, decreasing linearly on a logarithmic scale to value of zero within the range of the first four nodes of the computational grid. The left wall simulates a typical short-range wall of physical interaction potentials, and is intended to prevent the remnants of the wavepacket from intruding into the coordinate grid diapason from the left, and instead causing it to be reflected back from the right. As a quantitative characteristic of the absorbing efficiency in this model, we used the distortion coefficient $D = \int_{\{r\}} |\psi(r, t)|^2 dr$ where the integral spanned the entire range $\{r\}$ of the computational grid (equal to $(R + T)$, and in practice indistinguishable from the reflection coefficient R within the computational accuracy, thanks to the very short range of r and the very small amplitudes of the wavepacket behind the absorbing barrier). Fig. 2 illustrates the evolution of the wavepacket in this model, computed with our Fourier Grid package, in a similar way to Fig. 1.

Attention should be drawn to the fact that many of the values of R, T, D estimated in this way are so small that they are at the limits of computational accuracy. Consequently, they are very sensitive to computational details (grid characteristics, parameters of the initial Gaussian, etc.). We discovered that any change in these details could change these values as much as twice, or even more; this forced
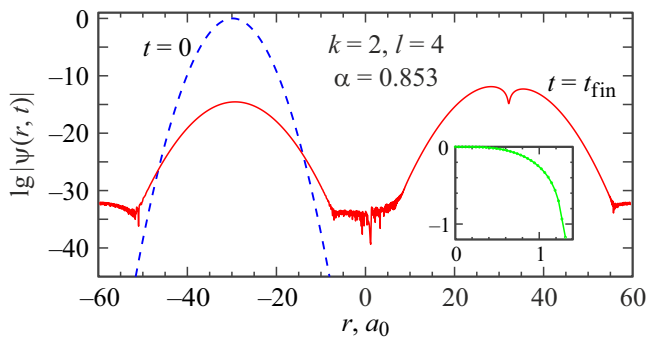
Figure 1. Decimal logarithms of wavepacket amplitudes at time instants $t = 0$ and t_{fin}, evolved using the model of Vibók and Balint–Kurti [33] with the cosine-type optical potential (Section 2.2) and $k = 2$, $l = 4$, and $\alpha = 0.853$ for a wavepacket with energy $E = E_0 = 0.1$ au. The absorbing region spans a length $\sim 1.3a_0$ (where a_0 is the Bohr radius) to the right of $r = 0$. The inset shows the imaginary part of the optical potential.
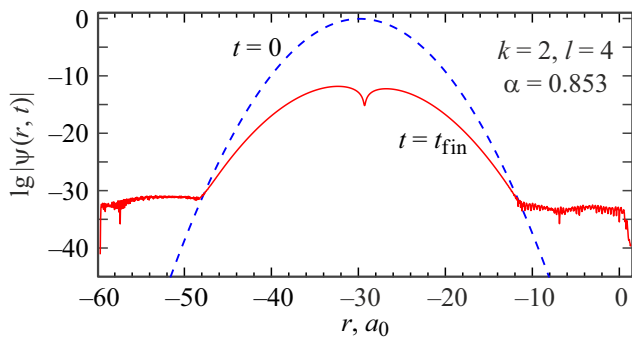

Figure 2. Decimal logarithms of wavepacket amplitudes at time instants $t = 0$ and t_{fin}, evolved in a model with an absorbing barrier to the right and a wall to the left, with a cosine-type optical potential (Section 2.2) for $k = 2$, $l = 4$, and $\alpha = 0.853$, for a wavepacket with energy $E = E_0 = 0.1$ au. The absorbing region spans a length $\sim 1.3a_0$ (where a_0 is the Bohr radius) to the right of $r = 0$.

us to choose a rather wasteful set of parameters to ensure the relative stability of our estimates. More specifically, for each wavepacket with mean energy E, we chose a grid with eight nodes per oscillation. The half-width of the Gaussian was equal to seven wavelengths of this oscillation. The center of the Gaussian at $t = 0$ was located in the center of the diapason, to the left of $r = 0$, spanning 26 Gaussian half-widths. In the model of Vibók and Balint–Kurti, the length of the grid to the right of $r = 0$ was also equal to 26 Gaussian half-widths, while in the model with an absorbing barrier to the right and a wall to the left, it was limited by the value of $(l + l_+)\lambda_0$ (the user-defined dimensionless length l spans the region where $z(r) \in [0, 1]$ and l_+ is the length of an extra absorbing zone behind it — see details in Sec. 4 below). The absorbing barrier was placed to the right of $r = 0$, and spanned a range of $(l + l_+)\lambda_0$ in both cases. The evolution time tfin was precomputed as the time required for the center of the freely evolved Gaussian to

move twice through the distance from its initial location to $r = 0$. We would like to emphasize once again that the numerical estimates obtained in this manner should be not considered exact quantitative results but rather tendencies, which are primarily seen on a logarithmic scale.

Using the model of Vibók and Balint–Kurti, we performed a series of computations emulating those in [33], with the aim of determining the „optimal" parameters of the optical potentials to ensure minimal values of $(R + T)$ for a particular energy $E = E_0$. These computations were done for the optical potential in Eq. (6), with $k = 1, 2, 3, 4$ and $l = 1$ through $l = 15$, $l_+ = 0$. The results are presented in the first four columns (l, α, R, T) of Table 2. The fifth column D is the distortion coefficient, which was computed using the same parameters, in the model with an absorbing barrier to the right and a wall to the left. The last two columns are the results of a similar optimization to ensure minimal values of the distortion coefficient D in the latter model. It can be seen from this table that in comparison with the analogous tables in [33], the efficiency of our cosine-type optical potential is generally close to that in [33], and is somewhat better at longer l. The results for $k = 3$ almost totally surpass the results for the quartic optical potential recommended in [33], although in our opinion, all of the other results are also appropriate for most practical needs.

Fig. 3 illustrates the typical distortion properties of the optical potential in Eq. (6) for the models of Vibók and Balint–Kurti and our other model, and their dependence on the parameter α. It can be seen that in the region of relatively large α, both curves are similar to each other, although they diverge in the region of small α. As a consequence, the D-curve (in the second model) has two minima, the second of which is very close to the minimum of the $(R + T)$-curve (in the first model); however, the global minimum is located in the region of smaller α.

Usually, a range of energies E is of interest rather than a single value $E = E_0$, and it is desirable that the absorbing efficiency should remain high over this entire range. Figs. 4 and 5 show the distortion coefficient D (in the second model) computed for $k = 2$, $l = 4$, and values of α from Table 2, D-optimized (first minimum in Fig. 3) and $(R + T)$-optimized (second minimum in Fig. 3) for $E_0 = 0.1$ au in a range of energies $E = 0.01$ au to $E = 1$ au (indicated by circles connected by black solid lines). The D-optimized curve in Fig. 4 exhibits better efficiency at energies equal to or less than E_0, while the $(R + T)$-optimized curve in Fig. 5 is better at higher energies. This observation suggests a choice between these values of α depending on the energy range of interest.

The two other curves in Figs. 4 and 5 illustrate the effects of extending the absorbing range by a value $l_+ = 1$, as mentioned above and described in more detail in Sec. 4 below, and of including the real-type summand in Eq. (7) with $\gamma = 1$. As expected, the l_+-extension mechanism is able to reduce the distortion by several orders of magnitude at higher energies, while the real-type summand reduces

Table 2. Parameters of the cosine-type absorbing function/optical potential (Section 2.2) optimized for the minimal value of $(R + T)$ (where R is the reflection coefficient, and T is the transmission coefficient) using the model of Vibók and Balint–Kurti [33]kd , and parameters optimized for the minimal value of the distortion coefficient D in the model with an absorbing barrier to the right and a wall to the left. The character „e" represents the decimal order

l	$(R + T)$-optimized				D-optimized		$(R + T)$-optimized				D-optimized	
	α	R	T	D	α	D	α	R	T	D	α	D
	$k = 1$						$k = 2$					
1	1.17	5.4e-04	7.1e-04	7.3e-04	0.682	3.9e-06	0.697	1.2e-03	2.7e-03	2.6e-03	0.422	9.3e-04
2	2.10	5.6e-10	2.1e-06	2.1e-06	0.552	1.4e-06	0.691	2.6e-06	6.3e-06	6.3e-06	0.376	3.7e-07
3	0.805	7.7e-08	4.6e-07	4.6e-07	0.377	1.4e-07	0.708	4.5e-09	1.9e-08	1.9e-08	0.372	2.8e-10
4	0.638	1.3e-08	9.2e-08	9.2e-08	0.297	2.6e-08	0.853	3.6e-13	7.4e-11	7.4e-11	0.339	4.3e-11
5	0.531	3.3e-09	2.6e-08	2.6e-08	0.250	7.3e-09	0.567	2.0e-12	1.8e-11	1.8e-11	0.299	5.5e-12
6	0.456	1.1e-09	9.3e-09	9.3e-09	0.218	2.6e-09	0.488	2.8e-13	2.9e-12	2.9e-12	0.271	1.0e-12
7	0.401	4.3e-10	3.9e-09	3.9e-09	0.197	1.1e-09	0.427	5.8e-14	6.4e-13	6.4e-13	0.248	2.4e-13
8	0.358	1.9e-10	1.8e-09	1.8e-09	0.180	5.4e-10	0.381	1.4e-14	1.7e-13	1.7e-13	0.228	6.9e-14
9	0.324	9.7e-11	9.3e-10	9.3e-10	0.167	2.9e-10	0.343	4.4e-15	5.4e-14	5.4e-14	0.211	2.3e-14
10	0.297	5.0e-11	5.1e-10	5.1e-10	0.156	1.6e-10	0.313	1.5e-15	1.9e-14	1.9e-14	0.197	8.5e-15
11	0.274	2.8e-11	3.0e-10	3.0e-10	0.147	9.9e-11	0.288	5.6e-16	7.6e-15	7.6e-15	0.185	3.5e-15
12	0.255	1.6e-11	1.8e-10	1.8e-10	0.139	6.2e-11	0.267	2.3e-16	3.3e-15	3.3e-15	0.174	1.5e-15
13	0.238	1.1e-11	1.1e-10	1.1e-10	0.132	4.0e-11	0.249	9.9e-17	1.5e-15	1.5e-15	0.164	7.1e-16
14	0.224	6.6e-12	7.6e-11	7.6e-11	0.126	2.7e-11	0.233	4.9e-17	7.2e-16	7.2e-16	0.156	3.5e-16
15	0.211	4.5e-12	5.1e-11	5.1e-11	0.121	1.9e-11	0.220	2.2e-17	3.7e-16	3.7e-16	0.148	1.8e-16
	$k = 3$						$k = 4$					
1	0.483	2.0e-03	5.0e-03	4.8e-03	0.298	2.8e-03	0.249	3.7e-03	3.2e-03	4.9e-03	0.101	2.0e-03
2	0.468	8.0e-06	1.8e-05	1.8e-05	0.193	2.1e-06	0.325	1.3e-05	2.7e-05	2.6e-05	0.146	1.9e-06
3	0.465	3.5e-08	7.6e-08	7.6e-08	0.215	2.2e-09	0.333	8.8e-08	1.7e-07	1.7e-07	0.164	1.8e-09
4	0.465	1.5e-10	3.3e-10	3.3e-10	0.266	8.4e-12	0.338	5.6e-10	1.1e-09	1.1e-09	0.186	2.7e-11
5	0.468	5.9e-13	1.6e-12	1.6e-12	0.295	5.0e-14	0.341	3.5e-12	7.1e-12	7.1e-12	0.218	2.2e-13
6	0.489	9.4e-16	1.2e-14	1.2e-14	0.306	2.3e-15	0.343	2.2e-14	4.6e-14	4.6e-14	0.237	1.6e-15
7	0.528	4.3e-19	8.0e-16	8.0e-16	0.279	3.3e-16	0.344	1.4e-16	3.0e-16	3.0e-16	0.250	1.2e-17
8	0.391	9.0e-18	1.2e-16	1.2e-16	0.255	5.4e-17	0.346	8.4e-19	2.4e-18	2.4e-18	0.258	1.9e-19
9	0.353	1.6e-18	2.3e-17	2.3e-17	0.236	1.1e-17	0.347	5.2e-21	5.5e-20	5.5e-20	0.254	1.9e-20
10	0.322	3.4e-19	5.3e-18	5.3e-18	0.219	2.7e-18	0.323	4.0e-22	5.6e-21	5.6e-21	0.234	3.1e-21
11	0.296	8.7e-20	1.4e-18	1.4e-18	0.205	7.3e-19	0.300	5.7e-23	9.9e-22	9.9e-22	0.219	5.6e-22
12	0.274	2.5e-20	4.2e-19	4.2e-19	0.192	2.2e-19	0.279	9.9e-24	2.1e-22	2.1e-22	0.204	1.2e-22
13	0.255	7.9e-21	1.4e-19	1.4e-19	0.181	7.6e-20	0.258	2.6e-24	5.0e-23	5.0e-23	0.193	2.9e-23
14	0.238	2.6e-21	5.0e-20	5.0e-20	0.171	2.8e-20	0.240	4.4e-25	1.4e-23	1.3e-23	0.182	7.8e-24
15	0.225	1.1e-21	1.9e-20	1.9e-20	0.163	1.1e-20	0.228	2.7e-25	3.8e-24	3.8e-24	0.171	2.3e-24

the distortion by about one order of magnitude at lower energies.

Modern spectroscopic experiments on the PA of ultracold atoms via magnetically tuned near-dissociation Feshbach resonances (see [18] and references therein) require a description of the Feshbach resonances at very low energies, corresponding to very long oscillation lengths (several hundreds of Bohr radii or even more). The numerical tests presented in Table 2 were done with lengths of the absorption zone of no less than the oscillation length, which required dealing with very long zones to simulate these near-dissociation features. It can be observed that the efficiency of the short $(l = 1)$ absorption zones is higher for smaller k, meaning that they are more promising for these types of problem. In order to explore how short the absorption zone can be, we carried out the following computation. For $k = 1$ and $l = 1$, with the same reference energy $E_0 = 0.1$ au, we computed the distortion coefficients for wavepackets with 10 equally spanned energies, $E = 0.01$ au through $E = 0.1$ au, and optimized the parameters α and γ to obtain the least possible distortion in all 10 cases using the least squares fit (LSF). The final LSF-optimized values were $\alpha = 0.311$ and $\gamma = 0.432$. This result was compared with the results of computations with the D-optimized $\alpha = 0.682$ from Table 2 and $\gamma = 0$, $\gamma = 1$ in Fig. 6. The LSF-optimization made the distortion coefficients more uniform, somewhat improving the region of smaller energies but worsening the region of higher energies. For energies noticeably lower than the ones shown in Fig. 6, we were unable to get reasonably small
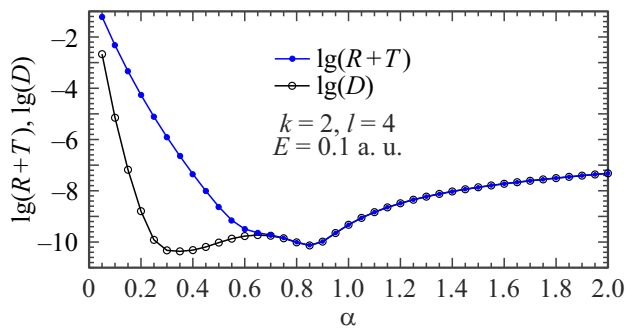
Figure 3. Decimal logarithms of the sum $(R + T)$ of the reflection R and transmission T coefficients in the model of Vibók and Balint–Kurti [33], and of the distortion coefficient D in the model with an absorbing barrier to the right and a wall to the left *vs.* the parameter α of the cosine-type optical potential (Section 2.2), for $k = 2$, $l = 4$ for a wavepacket with the energy $E = E_0 = 0.1$ au.
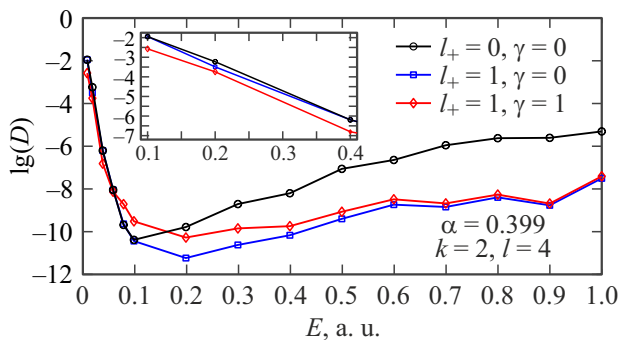

Figure 4. Decimal logarithms of the distortion coefficients D in the model with an absorbing barrier to the right and a wall to the left vs. the energy of the wavepacket computed with the cosine-type optical potential (Section 2.2), for $k = 2$, $l = 4$, and $\alpha = 0.399$ optimized for minimal D with energy $E_0 = 0.1$ au: the pure optical potential and the potential corrected by extending absorbing region to the right by a length $l_+ = 1$ and by including the real-type summand with depth $\gamma = 1$. The inset shows a magnified view of the leftmost part of the graph.

distortion coefficients, and the values remained $D \sim 1$. For the smallest $E = 0.01$ au, the length of the absorption zone was $\sqrt{10} \approx 3.2$ times shorter than the oscillation length. Hence, we can conclude that an appropriate choice for the absorbing function parameters can enable us to use the absorption zone with length as short as $\sim 1/3$ of the oscillation length with a characteristic accuracy of several percent.

4.   Software Implementation

Briefly, the Fourier Grid method involves the obvious, simple forms of the differentiation operators p (momentum) and K (kinetic energy) in the momentum representation. Fourier-based estimates of differentiation operators have much a higher accuracy than finite-difference approximations, and this allows us to employ much smaller compu-

tational grids. The inverse Fourier transforms of K and p from the momentum to the coordinate representation can be expressed as matrices with compact analytical forms [21,30].

By summing K with the matrix U of the potential energy (not excluding the case of several interacting channels), we obtain a coordinate grid representation of the Hamiltonian matrix H, which can then be diagonalized with standard methods of computational mathematics or exponentiated (in the matrix sense) to get the evolution operator $T(t) = \exp(-iHt/\hbar)$, thus enabling the evolution of the wavepacket $\psi(t)$ to be computed in a single time step t.

One of the strongest advantages of the Fourier Grid method is its ability to work with non-equidistant grids (the Mapped Fourier Grid method [21,30,49]), which can be constructed („optimized") to give fewer nodes in ranges of coordinates where the momenta of the wavepackets are small, thus making the overall grids much more compact. In constructing of either the equidistant or mapped grids, an existence of an upper boundary energy $\mathscr{E}$ is implied, so that the wavefunctions of the states below $\mathscr{E}$ are to be correctly represented on those grids.

For the most part, our realization of the Fourier Grid method as a software program follows this ideas and implements most of the features described in the original articles [26–32]. The most significant difference is that its interface is adapted for use with our Optimizer package.

The Optimizer package was presented for the first time at the conference in Ref. [50] (even though we had used earlier versions for at least two decades beforehand, see the terminal paragraph of this section). The open-source Matlab codes and all the application programs (including those described in the present article) are available from [21]. This package provides elaborate tools for the block-by-block construction and optimization of general mathematical and physical models. The main method of (generally nonlinear) optimization is the Levenberg. Marquardt method [51,52], which is based on Singular Value Decomposition (SVD) [53] of the local design (Jacobi) matrix. Many regularization tools are included, such as robust estimators that can be used instead of the default Least Squares Fit (LSF) approach, truncated SVD (Principal Component Regression, PCR), Tikhonov regularization (Ridge Regression, RR), etc. Parallel computations are supported. Other features and regulations are detailed in the manuals, which are also available from [21].

The (Mapped) Fourier Grid program is written entirely in Matlab. It is capable of constructing the Hamiltonian matrix, and diagonalizing it (i.e., finding eigenenergies and eigenfunctions) using the Matlab functions „eig" (a traditional diagonalization method) or .eigs. (the Lanczos method [54,55]). Further details of these are available from the Matlab help system and the program manuals. It can also compute the rotational constants and the multichannel component fractions (fractional partitions) for each eigenstate. The potential $U(r)$ is provided as a vector (in the one-channel case) or a matrix (in the multi-channel case) in a diabatic representation on a spatial grid.
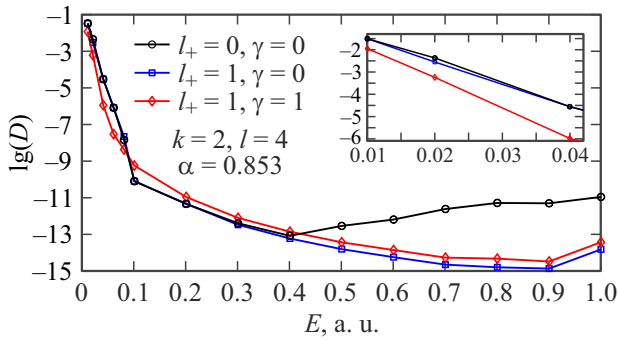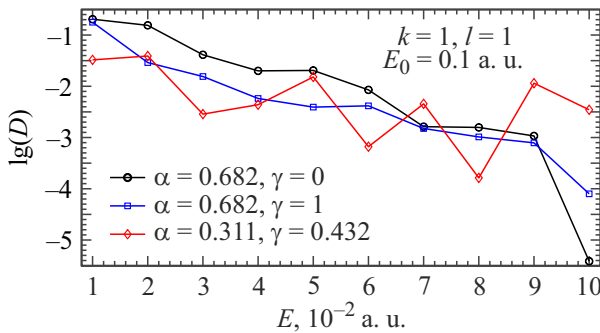
Figure 5. Decimal logarithms of the distortion coefficients D in the model with an absorbing barrier to the right and a wall to the left vs. the energy of the wavepacket computed with the cosine-type optical potential (Section 2.2), for $k = 2$, $l = 4$, and $\alpha = 0.853$ optimized for the minimal sum $(R + T)$ of the reflection R and transmission T coefficients with energy $E_0 = 0.1$ au: the pure optical potential and the potential corrected by extending the absorbing region to the right by a length $l_+ = 1$ and by including the real-type summand with depth $\gamma = 1$. The inset shows a magnified view of the leftmost part of the graph.

Figure 6. Decimal logarithms of the distortion coefficients D in the model with an absorbing barrier to the right and a wall to the left vs. the energy of the wavepacket computed with the cosine-type optical potential (Section 2.2), for $k = 1$, $l = 1$, and α optimized for minimal D with energy $E_0 = 0.1$ au (circles indicate $\gamma = 0$ and squares $\gamma = 1$) and a set of α and γ LSF-optimized for minimal values of equally weighted D over the entire range shown.

The main program does not include any damping tool, so the optical potential (if needed) must be included in the potential $U(r)$ before being passed to the main program. An extra Matlab function is provided to enable the inclusion of the optical potential in the form of Eq. 8, with the user-defined parameters k, α, γ, and the boundaries of the range of action of the optical potential. In addition to considering the absorption region within the range of the length $l\lambda_0$ (where l is a user-defined dimensionless length in units of the oscillation length $\lambda_0 = 2\pi\hbar/\sqrt{2mE_0}$ for some reference energy E_0) corresponding to $z \in [0, 1]$ (i.e., the r-scale interval with the boundaries corresponding to $\min(r)$ and $\max(r)$ of Sec. 2.2), we consider a possible change in this range to a length $(l + l_+)\lambda_0$; for $l_+ > 0$, this implies the

inclusion of a region with $z > 1$, where in the step-by-step scheme, the wavefunction is multiplied by zero.

An optimal mapped grid (if needed) is also constructed using a separate Matlab function with any predefined envelope potential [21,30,49] $V(r)$ (generally, can differ from the physical potential $U(r)$).

Other novelties distinguishing our realization of the Forier Grid method from the earlier ones are outlined below.

In the mapped-coordinate representation, the Hamiltonian $H = K + U$ is transformed to: [21,30,49]

$$\tilde{H} = \tilde{K} + U = -\frac{\hbar^2}{2m} \left(\sqrt{\frac{dx}{dr}} \left[\frac{d}{dx} \right] \sqrt{\frac{dx}{dr}} \right)^2 + U, \quad (9)$$

where r is the physical spatial coordinate and x is the mapped coordinate.

In other implementations of the Mapped Fourier Grid method (e.g., [30,32]), the commutations of the differentiation operator $[d/dx]$ and the square root $\sqrt{dx/dr}$ of the Jacobi matrix are done explicitly in a form of analytical equations, in order to get the operator $[d^2/dx^2]$, which results in arising of the second derivatives d^2x/dr^2. We do not see a need to do this, since Eq. (9) can easily be computed directly as a matrix expression, especially with the highly efficient matrix algebra of Matlab. Besides, when carrying out the iterative optimizing computations, there is no need to recompute the matrix $\tilde{K}$ of the kinetic energy (as well as the mapped coordinate) at each subsequent iteration, and in the multichannel case, this matrix remains the same for every channel.

A further novel aspect is the use of the r-dependent upper-boundary energy $\mathscr{E}$ to construct the „optimal" grid [21,30,49]. Indeed, there is no formal reason for keeping its value constant over the entire region, and an appropriate dependence on r can noticeably reduce the number of the spatial grid nodes without inflicting the physical mechanisms. We chose a dependence in the form

$$\mathscr{E}(r) = [V(r_r) + d\mathscr{E}_r] + [(V(r_l) + d\mathscr{E}_l)$$
$$- (V(r_r) + d\mathscr{E}_r)] \exp\left[-\epsilon \frac{r - r_l}{r_r - r_l}\right], \quad (10)$$

where r_l and r_r are the left and the right boundaries of the coordinate grid, implying $V(r_l) > V(r_r)$ (or, more exactly, $V(r_l) + d\mathscr{E}_l > V(r_r) + d\mathscr{E}_r$ — see below). The parameter ϵ determines the rate of decrease of this function from left to right; in many of the test computations, the value $\epsilon = 25$ was shown to be reasonable. The quantities $d\mathscr{E}_l$ and $d\mathscr{E}_r$ are needed to exclude artificial features at the boundaries. [For $d\mathscr{E}_l = 0$ and $d\mathscr{E}_r = 0$, all the off-diagonal boundary elements of the Hamiltonian matrix $\tilde{H}$ in the mapped-coordinate representation Eq. 9 are zero with $V(r) = \mathscr{E}$, and the formal non-physical solution of the eigenvalue problem would be one where the boundary element of the eigenvector is the only nonzero element and the eigenvalue is equal to the value of the potential at this boundary point — see details in‘[21].] Small values of these

quantities (relative to the characteristic energy scale of the problem) do not increase the computational grid noticeably. In the case where $V(r_l) + d\mathscr{E}_l \leq V(r_r) + d\mathscr{E}_r$, the constant value $V(r_r) + d\mathscr{E}_r$ is taken as E.

In a technical implementation of the optical potential method, a difficulty emerges from Eq. 6 for points with very small (close to zero) values of the function $f_{k1}(z(r))$, whose natural logarithms tend to minus infinity. Although Matlab allows us to work with the object Inf, some operations are unavailable and some are not quite correct with this object. For example, the eigenvalues and eigenvectors of a matrix containing elements of the Inf type cannot be computed. These values turn to minus infinity rather abruptly, so that the finite values before this occurs have quite reasonable magnitudes, although with very small magnitudes of their exponents. To overcome this drawback, we used a straightforward linear approximation from the last finite values of the optical potential in Eq. 6; in the case where this linear approximation also turns computationally to $-\text{Inf}$ (although we did not encounter this situation in practice), it is set to the last finite value computed. This should clarify how the extension of the absorption region to $l + l_+$ is realized in practice, in terms of the optical potential.

When the Hamiltonian matrix has been computed in the main (Mapped) Fourier Grid program, the evolution operator can be computed with the help of the inbuilt Matlab function „expm" for matrix exponentiation, and the evolution of the wavepacket $\psi(t)$ can be found. A separate Matlab program to calculate this is also provided.

In [30], an algorithm was proposed to interpolate the computed wavefunction from a relatively thin grid to any desired point in the coordinate space. This algorithm was based on the general properties of the Fourier transform, and can be applied with the utmost possible efficiency. However, we would like to emphasize that in most cases, this interpolation is not needed, since all the quantum-mechanical matrix elements can be computed within the accuracy of the entire algorithm as sums (approximating the theoretically ideal integrals) over the grid. This is clear from the reformulation of the infinite-dimensional quantum-mechanical perturbation theory in terms of the finite-dimensional Hamiltonian matrix used in the computations. In particular, the values of the rotational constants and the multichannel component fractions (fractional partitions) are computed this way in our programs.

We have extensively used earlier versions of the programs described here in our research. Some examples of the applications of our Fourier Grid programs to problems in molecular spectroscopy can be found in, e.g., [2,56,57]. The downloadable package (see Ref. [21]) contains a reproducible sample model able to adequately calculate the rovibrational structure in the blended complex $A^1\Sigma_u^+ \sim b^3\Pi_u$ of the rubidium dimer within a rather complicated 3-channel model of Ref. [58]. The Optimizer package has been used more widely in numerous applications (see [3,59–90] and the references therein).

5. Conclusions

Summing up, we propose the use of an absorbing function/optical potential formed from a combination of cosines in quantum-mechanical calculations of the spectroscopic and scattering properties of a two-body (e. g., diatomic) system. This type of function is able to ensure a high degree of smoothness of the joints with the physically substantive region. We present a software implementation of the (Mapped) Fourier Grid method, and describe its particular qualities. Tests of the cosine-type optical potential were done using our Fourier Grid program, and the good efficacy of this optical potential was demonstrated. These numerical tests showed that reducing the length of the absorbing zone to $\sim 1/3$ of the wavefunction oscillation length (de Broglie wavelength) with the appropriate set of optical potential parameters leads to a characteristic inaccuracy of several percent.

Acknowledgements

References

[1] L.D. Landau, E.M. Lifshitz. *Quantum Mechanics. Non-Relativistic Theory* (Pergamon, Oxford–New York–Toronto–Sydney–Paris–Frankfurt, 1977). DOI: 10.1016/C2013-0-02793-4

[2] X. Wang, W. Liu, Y. Li, J. Wu, V.B. Sovkov, J. Ma, S. Onishchenko, P. Li, Y. Fu, D. Li, Q. Fan, L. Xiao, S. Jia. Physical Chemistry Chemical Physics, **22**, 3809 (2020). DOI: 10.1039/C9CP05870B

[3] J. Wu, W. Liu, X. Wang, J. Ma, D. Li, V.B. Sovkov, L. Xiao, S. Jia. Journal of Chemical Physics, **148**, 174304 (2018). DOI: 10.1063/1.5023330

[4] N. Zheng, W. Liu, V.B. Sovkov, J. Xu, G. Ge, Y. Li, P. Li, Y. Fu, J. Wu, J. Ma, L. Xiao, S. Jia. Optics Express, **29**(21), 32892 (2021). DOI: 10.1364/OE.437881

[5] M. Guo, B. Zhu, B. Lu, X. Ye, F. Wang, R. Vexiau, N. Bouloufa-Maafa, G. Quéméner, O. Dulieu, D. Wang. Physical Review Letters, **116**, 205303 (2016). DOI: 10.1103/PhysRevLett.116.205303

[6] X. Ye, M. Guo, M.L. González-Martínez, G. Quéméner, D. Wang. Science Advances, **4**, eaaq0083 (2018). DOI: 10.1126/sciadv.aaq0083

[7] N.Y. Yao, M.P. Zaletel, D.M. Stamper-Kurn, A. Vishwanath. Nature Physics, **14**, 405 (2018). DOI: 10.1038/s41567-017-0030-7

[8] N. Goldman, J.C. Budich, P. Zoller. Nature Physics, **12**, 639 (2016). DOI: 10.1038/nphys3803

[9] N.R. Cooper, G.V. Shlyapnikov. Physical Review Letters, **103**, 155302 (2009). DOI: 10.1103/PhysRevLett.103.155302

[10] J.L. Bohn, A.M. Rey, J. Ye. Science, **357**, 1002 (2017). DOI: 10.1126/science.aam6299

[11] I. Kozyryev, N.R. Hutzler. Physical Review Letters, **119**, 133002 (2017). DOI: 10.1103/PhysRevLett.119.133002

[12] W.B. Cairncross, D.N. Gresh, M. Grau, K.C. Cossel, T.S. Roussy, Y. Ni, Y. Zhou, J. Ye, E.A. Cornell. Physical Review Letters, **119**, 153001 (2017). DOI: 10.1103/PhysRevLett.119.153001

[13] J. Kobayashi, A. Ogino, S. Inouye. Nature Communications, **10**, 3771 (2019). DOI: 10.1038/s41467-019-11761-1

[14] S.A. Moses, J.P. Covey, M.T. Miecnikowski, D.S. Jin, J. Ye. Nature Physics, **13**(1), 13 (2017). DOI: 10.1038/nphys3985

[15] D. DeMille. Physical Review Letters, **88**, 067901 (2002). DOI: 10.1103/PhysRevLett.88.067901

[16] N.V. Vitanov, A.A. Rangelov, B.W. Shore, K. Bergmann. Reviews of Modern Physics, **89**, 015006 (2017). DOI: 10.1103/RevModPhys.89.015006

[17] K. Bergmann, H. Theuer, B.W. Shore. Reviews of Modern Physics, **70**, 1003 (1998). DOI: 10.1103/RevModPhys.70.1003

[18] G. Feng, Y. Li, X. Wang, J. Wu, V.B. Sovkov, J. Ma, L. Xiao, S. Jia. Scientific Reports, **7**, 13677 (2017). DOI: 10.1038/s41598-017-13534-6

[19] Y. Li, X. Wang, J. Wu, G. Feng, W. Liu, V.B. Sovkov, J. Ma, B. Deb, L. Xiao, S. Jia. Physical Chemistry Chemical Physics, **23**(1), 641 (2021). DOI: 10.1039/D0CP04840B

[20] J.G. Muga, J.P. Palao, B. Navarro, I.L. Egusquiza. Physics Reports, **395**, 357 (2004). DOI: 10.1016/j.physrep.2004.03.002

[21] V.B. Sovkov. *Optimizer: source codes and manuals & collection of applications, 2019–2022.* URL: https://sourceforge.net/projects/optimizer-sovkov/

[22] I. Schaefer, R. Kosloff. Physical Review A: Atomic, Molecular, and Optical Physics, **101**, 023407 (2020). DOI: 10.1103/PhysRevA.101.023407

[23] B. Schmidt, U. Lorenz. Computer Physics Communications, **213**, 223 (2017). DOI: 10.1016/j.cpc.2016.12.007

[24] B. Schmidt, C. Hartmann. Computer Physics Communications, **228**, 229 (2018). DOI: 10.1016/j.cpc.2018.02.022

[25] B. Schmidt, R. Klein, L.C. Araujo. Journal of Computational Chemistry, **40**, 2677 (2019). DOI: 10.1002/jcc.26045

[26] D. Kosloff, R. Kosloff. Journal of Computational Physics, **52**, 35 (1983). DOI: 10.1016/0021-9991(83)90015-3

[27] J.C. Light, I.P. Hamilton, J.V. Lill. Journal of Chemical Physics, **82**, 1400 (1985). DOI: 10.1063/1.448462

[28] C.C. Martson, G.G. Balint-Kurti. Journal of Chemical Physics, **91**, 3571 (1989). DOI: 10.1063/1.456888

[29] D. Neuhasuer, M. Baer. Journal of Chemical Physics, **90**, 4351 (1989). DOI: 10.1063/1.456646

[30] V. Kokooouline, O. Dulieu, R. Kosloff, F. Masnou-Seeuws. Journal of Chemical Physics, **110**, 9865 (1999). DOI: 10.1063/1.478860

[31] D. Lemoine. Chemical Physics Letters, **320**, 492 (2000). DOI: 10.1016/S0009-2614(00)00269-4

[32] K. Willner, O. Dulieu, F. Masnou-Seeuws. Journal of Chemical Physics, **120**, 548 (2004). DOI: 10.1063/1.1630031

[33] Á. Vibók, G.G. Balint-Kurti. Journal of Physical Chemistry, **96**, 8712 (1992). DOI: 10.1021/j100201a012

[34] Á. Vibók, G.G. Balint-Kurti. Journal of Chemical Physics, **96**, 7616 (1992). DOI: 10.1063/1.462414

[35] U.V. Riss, H.-D. Meyer. Journal of Chemical Physics, **105**, 1409 (1996). DOI: 10.1063/1.472003

[36] J.-Yuan Ge, J.Z.H. Zhang. Journal of Chemical Physics, **108**, 1429 (1998). DOI: 10.1063/1.475514

[37] J.G. Muga, B. Navarro. Chemical Physics Letters, **390**, 454 (2004). DOI: 10.1016/j.cplett.2004.04.059

[38] G.J. Halász, Á Vibók. Chemical Physics Letters, **323**, 287 (2000). DOI: 10.1016/S0009-2614(00)00487-5

[39] Á. Vibók, G.J. Halász. Physical Chemistry Chemical Physics, **3**, 3048 (2001). DOI: 10.1039/B101900G

[40] S. Kallush, R. Kosloff. Chemical Physics Letters, **433**, 221 (2006). DOI: 10.1016/j.cplett.2006.11.040

[41] R.E. Wyatt, B.A. Rowland. Journal of Chemical Theory and Computation, **5**, 443 (2009). DOI: 10.1021/ct800248w

[42] Y.-C. Han, K.-J. Yuan, W.-H. Hu, S.-L. Cong. Journal of Chemical Physics, **130**, 044308 (2009). DOI: 10.1063/1.3067921

[43] Y.-C. Han. International Journal of Quantum Chemistry, **119**, e25858 (2019). DOI: 10.1002/qua.25858

[44] E.W.F. Smeets, G. Füchsel, G.-J. Kroes. Journal of Physical Chemistry C, **123**, 23049 (2019). DOI: 10.1021/acs.jpcc.9b06539

[45] X. Antoine, A. Arnold, C. Besse, M. Ehrhardt, A. Schädle. Communications in Computational Physics, **4**(4), 729 (2008). URL: http://global-sci.org/intro/article_detail/cicp/7814.html

[46] A. Scrinzi. Physical Review A, **81**, 053845 (2010). DOI: 10.1103/PhysRevA.81.053845

[47] M. Weinmüller, M. Weinmüller, J. Rohland, A. Scrinzi. Journal of Computational Physics, **333**, 199 (2017). DOI: 10.1016/j.jcp.2016.12.029

[48] J. Kaye, L. Greengard. *Transparent boundary conditions for the time-dependent Schrödinger equation with a vector potential, 2019.* URL: https://arxiv.org/abs/1812.04200

[49] E. Fattal, R. Baer, R. Kosloff. Physical Review E, **53**, 1217 (1996). DOI: 10.1103/PhysRevE.53.1217

[50] V.B. Sovkov, J. Ma. In: *Proceedings of the 2016 International Conference on Applied Mathematics, Simulation and Modelling*, ed. by A. Dadvand, K.V. Nagaraja, M. Mirzazadeh. Advances in Computer Science Research (Atlantis Press, Beijing, China, 2016), vol. 41, p. 369 (No. 083). DOI: 10.2991/amsm-16.2016.83

[51] K. Levenberg. Quarterly of Applied Mathematics, **2**, 164 (1944).

[52] D.W. Marquardt. Journal of the Society for Industrial and Applied Mathematics, **11**, 431 (1963). DOI: 10.1137/0111030

[53] G.H. Golub, C.F. van Loan. *Matrix Computations* (The John Hopkins University Press, Baltimore and London, 1996). URL: https://jhupbooks.press.jhu.edu/content/matrix-computations

[54] C. Lanczos. Journal of Research of the National Bureau of Standards, **45**, 255 (1950). DOI: 10.6028/jres.045.026

[55] R.B. Lehoucq, G.G. Gray, D.-H. Zhang, J.-C. Light. Computer Physics Communications, **109**, 15 (1998). DOI: 10.1016/S0010-4655(98)00002-2

[56] V.B. Sovkov, F. Xie, D. Li, S.S. Lukashov, V.V. Baturo, J. Ma, L. Li. AIP Advances, **8**, 125322 (2018). DOI: 10.1063/1.5055675

[57] S.S. Onishchenko, V.B. Sovkov, F. Xie, D. Li, S.S. Lukashov, V.V. Baturo, J. Wu, J. Ma, L. Li. Journal of Quantitative Spectroscopy and Radiative Transfer, **250**, 107037 (2020). DOI: 10.1016/j.jqsrt.2020.107037

[58] A.N. Drozdova, A.V. Stolyarov, M. Tamanis, R. Ferber, P. Crozet, A.J. Ross. Physical Review A: Atomic, Molecular, and Optical Physics, **88**(2), 022504 (2013). DOI: 10.1103/PhysRevA.88.022504

[59] X. Wang, W. Liu, J. Wu, V.B. Sovkov, J. Ma, P. Li, L. Xiao, S. Jia. Journal of Quantitative Spectroscopy and Radiative Transfer, **240**, 106678 (2020). DOI: 10.1016/j.jqsrt.2019.106678

[60] P.T. Arndt, V.B. Sovkov, J. Ma, X. Pan, D.S. Beecher, J.Y. Tsai, Y. Guan, A.M. Lyyra, E.H. Ahmed. Physical Review A: Atomic, Molecular, and Optical Physics, **99**, 052511 (2019). DOI: 10.1103/PhysRevA.99.052511

[61] P.T. Arndt, V.B. Sovkov, J. Ma, X. Pan, D.S. Beecher, J.Y. Tsai, Y. Guan, A.M. Lyyra, E.H. Ahmed. Journal of Chemical Physics, **149**, 224303 (2018). DOI: 10.1063/1.5058282

[62] G. Feng, F. Xie, V.B. Sovkov, J. Ma, L. Xiao, S. Jia. Journal of the Physical Society of Japan, **87**, 024303 (2018). DOI: 10.7566/JPSJ.87.024303

[63] V.B. Sovkov, F. Xie, A.M. Lyyra, E.H. Ahmed, J. Ma, S. Jia. Journal of Chemical Physics, **147**, 104301 (2017). DOI: 10.1063/1.5001481

[64] V.B. Sovkov, F. Xie, A.M. Lyyra, E.H. Ahmed, J. Ma, S. Jia. Journal of Chemical Physics, **149**, 239901 (2018). DOI: 10.1063/1.5083024

[65] W. Liu, J. Wu, J. Ma, P. Li, V.B. Sovkov, L. Xiao, S. Jia. Physical Review A: Atomic, Molecular, and Optical Physics, **94**, 032518 (2016). DOI: 10.1103/PhysRevA.94.032518

[66] J. Yang, Y. Guan, W. Zhao, Z. Zhou, X. Han, J. Ma, V.B. Sovkov, V.S. Ivanov, E.H. Ahmed, A.M. Lyyra, X. Dai. Journal of Chemical Physics, **144**, 024308 (2016). DOI: 10.1063/1.4939524

[67] P.G. Volkov, S.I. Korobeinikov, V.I. Nikolaev, V.B. Sovkov. Journal of Analytical Chemistry, **71**(5), 471 (2016). DOI: 10.1134/S1061934816030151

[68] W. Liu, R. Xu, J. Wu, J. Yang, S.S. Lukashov, V.B. Sovkov, X. Dai, J. Ma, L. Xiao, S. Jia. Journal of Chemical Physics, **143**, 124307 (2015). DOI: 10.1063/1.4931646

[69] V.B. Sovkov, V.S. Ivanov. Journal of Chemical Physics, **140**, 134307 (2014). DOI: 10.1063/1.4869981

[70] V.B. Sovkov, V.S. Ivanov. Vestnik St. Petersburg University. Ser. 4, **1**(59), 473 (2014). URL: http://elibrary.ru/item.asp?id=22697447

[71] J. Ma, W. Liu, J. Yang, J. Wu, W. Sun, V.S. Ivanov, A.S. Skublov, V.B. Sovkov, X. Dai, S. Jia. Journal of Chemical Physics, **141**, 244310 (2014). DOI: 10.1063/1.4904265

[72] V.B. Sovkov, D. Li, V.S. Ivanov, A.S. Skublov, F. Xie, Li Li, S. Magnier. Chemical Physics Letters, **557**, 66 (2013). DOI: 10.1016/j.cplett.2012.12.030

[73] V.B. Sovkov, V.S. Ivanov, K.V. Minaev, M.S. Aleksandrov. Optics and Spectroscopy, **114**(2), 167 (2013). DOI: 10.1134/S0030400X13020288

[74] Y. Guan, X. Han, J. Yang, Z. Zhou, X. Dai, E.H. Ahmed, A.M. Lyyra, S. Magnier, V.S. Ivanov, A.S. Skublov, V.B. Sovkov. Journal of Chemical Physics, **139**, 144303 (2013). DOI: 10.1063/1.4823496

[75] F. Xie, Li Li, D. Li, V.B. Sovkov, K.V. Minaev, V.S. Ivanov, A.M. Lyyra, S. Magnier. Journal of Chemical Physics, **135**, 024303 (2011). DOI: 10.1063/1.3606397

[76] F. Xie, K.V. Minaev, V.B. Sovkov, V.S. Ivanov, D. Li, Li Li. Chemical Physics Letters, **493**, 238 (2010). DOI: 10.1016/j.cplett.2010.05.060

[77] F. Xie, V.B. Sovkov, A.M. Lyyra, D. Li, S. Ingram, J. Bai, V.S. Ivanov, S. Magnier, Li Li. Journal of Chemical Physics, **130**, 051102 (2009). DOI: 10.1063/1.3075580

[78] Bediha Beser, V.B. Sovkov, J. Bai, E.H. Ahmed, C.C. Tsai, F. Xie, Li Li, V.S. Ivanov, A.M. Lyyra. Journal of Chemical Physics, **131**, 094505 (2009). DOI: 10.1063/1.3194290

[79] F. Xie, D. Li, L. Tyree, L. Li, V.B. Sovkov, V.S. Ivanov, S. Magnier, A.M. Lyyra. Journal of Chemical Physics, **128**, 204313 (2008). DOI: 10.1063/1.2920191

[80] D. Li, F. Xie, Li Li, V.B. Sovkov, V.S. Ivanov, E. Ahmed, A.M. Lyyra, J. Huennekens, S. Magnier. Journal of Chemical Physics, **126**, 194314 (2007). DOI: 10.1063/1.2730804

[81] D. Li, F. Xie, Y. Chu, Li Li, S. Magnier, V.B. Sovkov, V.S. Ivanov. Chemical Physics, **332**, 10 (2007). DOI: 10.1016/j.chemphys.2006.11.018

[82] V.B. Sovkov, V.S. Ivanov, D. Li, F. Xie, Li Li. Optics and Spectroscopy, **103**(5), 723 (2007). DOI: 10.1134/S0030400X07110069

[83] F. Xie, D. Li, Y. Chu, Li Li, S. Magnier, V.B. Sovkov, V.S. Ivanov. Journal of Physical Chemistry A, **110**, 11260 (2006). DOI: 10.1021/jp063266m

[84] V.B. Sovkov, V.S. Ivanov, Li Li, Z. Chen, S. Magnier. Journal of Molecular Spectroscopy, **236**, 35 (2006). DOI: 10.1016/j.jms.2005.12.005

[85] E. Ahmed, A.M. Lyyra, F. Xie, D. Li, Y. Chu, Li Li, V.S. Ivanov, V.B. Sovkov, S. Magnier. Journal of Molecular Spectroscopy, **234**, 41 (2005). DOI: 10.1016/j.jms.2005.08.001

[86] E. Ahmed, A.M. Lyyra, Li Li, V.S. Ivanov, V.B. Sovkov, S. Magnier. Journal of Molecular Spectroscopy, **229**, 122 (2005). DOI: 10.1016/j.jms.2004.08.021

[87] P. Yi, X. Dai, J. Li, Y. Liu, Li Li, V.B. Sovkov, V.S. Ivanov. Journal of Molecular Spectroscopy, **225**, 33 (2004). DOI: 10.1016/j.jms.2004.02.005

[88] V.S. Ivanov, V.B. Sovkov, Li Li. Journal of Chemical Physics, **118**, 8242 (2003). DOI: 10.1063/1.1565107

[89] V.S. Ivanov, V.B. Sovkov, N. Gallice, Li Li, Y. Liu, A.M. Lyyra, S. Magnier. Journal of Molecular Spectroscopy, **209**, 116 (2001). DOI: 10.1006/jmsp.2001.8413

[90] V.S. Ivanov, V.B. Sovkov, Li Li, A.M. Lyyra, T.-J. Whang, S. Magnier. Journal of Chemical Physics, **114**, 6077 (2001). DOI: 10.1063/1.1355979